Macromolecules

pubs.acs.org/Macromolecules Article

Direct Observation of Ring Polymer Dynamics in the Flow-Gradient Plane of Shear Flow

Michael Q. Tu, Megan Lee, Rae M. Robertson-Anderson, and Charles M. Schroeder*

Cite This: *Macromolecules* 2020, 53, 9406–9419 Read Online

ACCESS | Metrics & More | Article Recommendations | Supporting Information

ABSTRACT: Ring polymers are a unique class of macromolecules that lack free ends and show qualitatively different dynamics compared to linear chains. Despite recent progress, the nonequilibrium flow behavior of ring polymers is not fully understood. In this work, we study ring polymer dynamics in steady shear flow using a combination of single molecule experiments and Brownian dynamics (BD) simulations. In particular, the dynamics of DNA ring polymers are studied in the flow-gradient plane of shear by using a custom flow apparatus that allows for direct observation of ring stretching and tumbling dynamics using single molecule fluorescence microscopy. Using this approach, we determined the average fractional polymer extension in the flow direction $\langle x \rangle / L_c$ and the average orientation angle with respect to the flow axis $\langle \theta \rangle$ for ring polymers in dilute solution shear flow as a function of dimensionless flow strength (Weissenberg number, *Wi*). In all cases, results for ring polymer dynamics are directly compared to linear chain counterparts. Interestingly, our results show that rings and linear chains exhibit similar average fractional extensions, orientation angle, and dimensionless gradient thickness over a wide range of flow strengths ($0 \leq Wi \leq 250$). However, ring polymers show qualitatively different probability distributions of molecular chain extension compared to linear chains in steady shear, which arises due to the circular chain architecture that limits the conformational phase space for rings. Power spectral densities of polymer orientation angle and cross-correlations between fractional chain extension and gradient-direction thickness are used to understand ring polymer tumbling behavior, enabling determination of tumbling frequency as a function of flow strength *Wi*. Cross-correlations are further used to understand differences in probability distributions of molecular chain extension between linear chains and rings in shear flow. Overall, these results provide a new understanding of the nonequilibrium dynamics of ring polymers in shear flow.

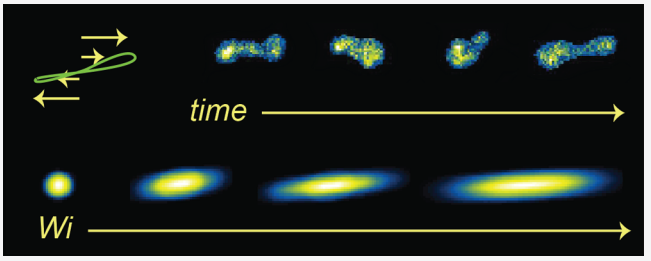

INTRODUCTION

Ring polymers have a unique nonlinear chain architecture that has fascinated polymer physicists and chemists for decades.[1,2] Ring polymers lack chain ends, which results in qualitatively different dynamics compared to linear and branched polymers.[3,4] In many cases, the physical properties of polymers are influenced by the chemical identity of chain termini,[5] yet ring polymers have no free ends and therefore defy classical theoretical descriptions used for linear or branched chain architectures. Ring polymers are ubiquitous in biology, where circular DNA plasmids are commonly used for molecular cloning applications and bacterial genomic DNA often occurs in circular form. Circular macromolecules are also playing a role in emerging biotechnologies, such as macrocyclic peptides for drug delivery applications.[6] In addition, synthetic polymers with circular topologies have recently been developed with unique supramolecular architectures, such as molecularly interlocked poly[*n*]catenanes.[7] Moreover, a synthetic circular polymer known as cyclic poly(phthalaldehyde) was recently shown to have robust mechanical properties while being susceptible to triggered degradation, thereby enabling new routes for recyclable materials.[8,9] Given the increasing importance of cyclic macromolecules, there is a clear need to understand their dynamics in flow.

In recent years, the rheological properties of ring polymer melts and solutions have been studied by using experiments and simulations.[10−14] Pioneering work on ring polystyrene melts revealed a reduced zero-shear viscosity for rings compared to linear polymers.[15,16] Following these early studies, new separation techniques based on liquid chromatography at the critical condition (LCCC) were developed, resulting in improved purities for ring polymer samples.[17] Using the LCCC purification method, researchers have studied the linear and nonlinear shear rheology of "pure-as-currently possible" ring polymer melts.[18,19] Interestingly, LCCC-purified ring polymer melts were shown to exhibit a power-law stress−relaxation behavior, which is qualitatively different than the

Received: June 9, 2020
Revised: October 9, 2020
Published: October 22, 2020

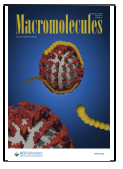

https://dx.doi.org/10.1021/acs.macromol.0c01362
Macromolecules 2020, 53, 9406−9419

stress−relaxation behavior of linear polymer melts and highly sensitive to trace amounts of linear polymer contamination.[18] The zero-shear viscosity of ring polymer melts has also been studied,[20] with prior work reporting some differences in the molecular weight scaling dependence and long-time relaxation behavior of LCCC-purified ring melts compared to theoretical predictions.[21] Recent work has focused on the nonlinear dynamics of LCCC-purified ring polymer melts in shear flow, revealing a transient stress overshoot in the start-up of simple shear.[22] In addition, nonlinear stress−relaxation experiments show that ring polymer melts exhibit a much weaker damping response compared to linear polymer melts and linear-doped ring polymer melt systems.[22] In 2019, uniaxial extensional rheometry experiments were reported on LCCC-purified ring polymer melts, revealing an unexpected tunable viscosity thickening and thinning.[23] Interestingly, densely entangled systems of ring polymers have been predicted to undergo a topological glass transition above a specific polymer molecular weight.[24−26]

Single molecule techniques allow for the direct observation of polymer dynamics in flow,[27] thereby providing a complementary set of experimental tools to understand the flow behavior and rheology of polymeric materials. Single polymer experiments on double-stranded DNA (dsDNA) have been extensively used to understand the equilibrium and nonequilibrium behavior of linear polymer chains. Dilute solution studies of linear chains have focused on polymer chain relaxation,[28] transient stretching dynamics in shear flow[29,30] and extensional flow,[31,32] and polymer conformation hysteresis.[33] Molecular rheology has been further used to study semidilute[34−36] and entangled solutions[37,38] of linear chains, with recent work revealing an unexpected double-mode relaxation behavior for entangled linear polymers.[38]

Recently, single molecule experiments have been extended to ring polymers, facilitated by perfectly monodisperse DNA-based ring polymers using plasmids and fosmids.[39] Prior work on equilibrium diffusion measurements has shown that ring polymers exhibit larger center-of-mass diffusion coefficients in dilute solution compared to their linear counterparts.[40,41] In addition, single DNA diffusion experiments in concentrated solutions have shown that the motion of individual ring polymers is greatly hindered in background solutions of linear chains compared to background solutions of rings due to intermolecular topological interactions.[42−44] The nonequilibrium stretching dynamics of rings in extensional flow has also been studied in dilute solution by using single molecule techniques, revealing a shifted coil−stretch transition and a less diverse set of transient stretching pathways compared to linear chain counterparts.[45] Interestingly, intramolecular hydrodynamic interactions (HI) were found to induce an open "looped" chain conformation for rings in the direction perpendicular to flow in planar extensional flow,[46] resulting in a shifted coil−stretch transition compared to linear chains. Recently, it was reported that ring polymers undergo large fluctuations in chain extension in semidilute solutions of linear chains in extensional flow.[47] Fluctuations in ring chain extension arise due to ring−linear threading events,[47] demonstrating the coupling between polymer chain architecture and intermolecular interactions in flow. Broadly speaking, the distinct molecular architecture of ring polymers confers a unique and rich set of dynamics that are not observed for linear polymers. However, prior single molecule experiments have mainly focused on ring polymer dynamics in extensional flow.[45−47]

Shear flow is ubiquitous and occurs any time a fluid moves past a stationary solid boundary. Shear flow is commonly encountered in processing applications such as solution-based coating flows.[48,49] In contrast to purely extensional flow, shear flow consists of equal parts of extension and rotation. In steady shear flow, linear polymers have been observed to continually undergo end-over-end tumbling motion, without reaching a stable steady-state conformation.[29,30,50−52] However, ring polymers are thought to exhibit qualitatively different dynamics in dilute solution shear flows due to a coupling between the circular chain architecture and flow vorticity. Prior computational studies of ring polymers in simple shear and linear mixed flows have shown that ring polymers exhibit a tumbling motion similar to linear polymers. However, unlike linear chains, ring polymers were reported to exhibit a tank-treading motion in steady shear, wherein the polymer backbone translates along its curvilinear contour.[53−56] From this view, although prior computational studies have reported interesting ring dynamics in shear, molecular-level experimental observations are lacking. Single molecule experiments would provide for the direct observation of ring polymers dynamics in shear flow.

In this work, we study the dynamics of DNA ring polymers in shear flow using single molecule experiments and Brownian dynamics (BD) simulations. Ring polymer dynamics are directly visualized in the flow-gradient plane of shear flow in dilute solution by using a custom-built flow apparatus suitable for fluorescence microscopy. Our results reveal a tumbling behavior of ring polymers in steady shear that is distinct from the canonical end-over-end tumbling motion of linear polymers due to the lack of chain ends. We further characterize the average fractional polymer extension $\langle x\rangle/L_c$, orientation angle $\langle\theta\rangle$, gradient-direction thickness $\langle\delta_2\rangle$, and distributions of molecular extension for rings in steady shear flow as a function of the dimensionless flow strength Weissenberg number, *Wi*. In addition, power spectral densities of polymer orientation angle and cross-correlations of polymer extension and gradient thickness are determined from BD simulations, and these quantities are used to determine tumbling frequencies for ring polymers in steady shear. In all cases, experimental results for ring polymers are directly compared to linear chain analogues. Overall, our work provides fundamentally new information regarding the dynamics of ring polymers in shear flow, thereby opening new avenues for relating dynamic microscopic chain conformation to bulk rheological behavior.

EXPERIMENTAL SECTION

Synthesis and Preparation of Ring DNA. A 114.8 kbp bacterial artificial chromosome (K16) was isolated by using standard cloning methods, as previously described.[39,41] Briefly, DNA constructs were extracted from *Escherichia coli* cells lysed by using an alkaline solution, and DNA was subsequently renatured using an acidic detergent solution. Genomic DNA and cellular debris precipitate were removed by centrifugation. Topoisomerase-I (New England Biolabs) was used to convert supercoiled DNA into relaxed circular form.[41]

Fluorescent Labeling and Preparation of DNA Solutions. K16 circular DNA (114.8 kbp) and linear λ-DNA (48.5 kbp, New England Biolabs) were fluorescently labeled with YOYO-1 dye (Invitrogen) at a 1:4 dye-to-bp ratio, as previously described.[47] Prior to labeling, λ-DNA was heated to 65°C for 10 min and snap-cooled to minimize concatemer formation due to complementary oligonucleotide overhangs. Fluorescently labeled K16 circular DNA (114.8 kbp)

https://dx.doi.org/10.1021/acs.macromol.0c01362
Macromolecules 2020, 53, 9406−9419

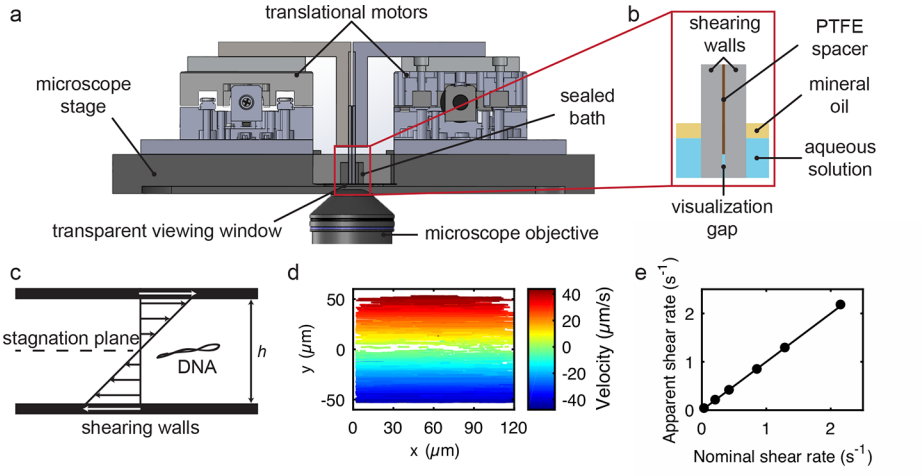

Figure 1. Flow apparatus for studying single polymer dynamics in the flow-gradient plane of shear. (a) Solidworks drawing (to scale) showing the custom shear apparatus mounted on the stage of an inverted microscope. Two motorized stages are mounted on an aluminum bath with an optical viewing window at the bottom that was sealed with a microscope coverslip. Two quartz microscope slides were affixed to the motorized stages and serve as the shearing surfaces. (b) Schematic (not to scale) showing a zoomed-in view of the device near the image area. The aqueous DNA solution was loaded into the device, and a PTFE spacer was used to maintain a constant gap between the shearing plates during experiments. A layer of mineral oil was added on top of the DNA solution to prevent evaporation. (c) Schematic showing DNA ring polymer dynamics in the flow-gradient plane of shear flow. (d) Particle tracking velocimetry (PTV) results showing the shear flow field at $\dot{\gamma} = 0.87\ s^{-1}$ with 0.84 μm diameter tracer particles. (e) Comparison between shear rates determined by using PTV and the nominal applied shear rates from the translational velocities of the shearing surfaces.

has a fully stretched contour length L_c = 24.9 μm corresponding to the circular chain conformation, which is equal to one-half of the contour length of the linear chain equivalent.[46] Fluorescently labeled linear λ-DNA (48.5 kbp) has a fully stretched contour length L = 21 μm.[27] DNA has a persistence length l_p = 53 nm in the buffered aqueous solutions used in these experiments,[27,57] yielding an overall number of Kuhn steps $N_k = 2L_c/b_k = 470$ for K16 circular DNA (full circular DNA backbone) and $N_k = L/b_k = 198$ for linear λ-DNA, where the Kuhn step size is $b_k = 2l_p$ for DNA.[58]

Fluorescently labeled DNA was diluted to a concentration $\approx 10^{-5}c^*$ in a buffered sucrose solution, where c^* is the polymer overlap concentration. The sucrose imaging buffer contained 5 mM NaCl, 30 mM Tris-HCl (pH 8.0), 2 mM EDTA, 5 mg/mL glucose, 1% v/v β-mercaptoethanol (Sigma), and 0.25 μg/mL glucose oxidase and 0.13 μg/mL catalase (Sigma) as oxygen scavengers to minimize photobleaching.[59] To enable imaging in the shear flow apparatus, the concentration of sucrose was carefully tuned by adding small amounts of water to match the refractive index of the polymer solution to that of quartz (n_D = 1.4585 ± 0.0002), as determined by using a refractometer (VeeGee Scientific). The concentration of sucrose in the imaging solutions was 67.1% w/w, and the solution viscosity was 0.23 Pa·s at 20.5 °C, determined by using a cone-and-plate viscometer (Brookfield). The solution was gently mixed on a rotating mixer (4 rpm) for ≥30 min before performing single molecule imaging experiments.

Shear Flow Device for Flow-Gradient Plane Imaging. A custom flow-gradient shear apparatus was designed and built to visualize the dynamics of single polymers in the flow-gradient plane (Figure 1). Although a few prior studies have used flow-gradient imaging devices coupled with fluorescence microscopy,[30,60] our device differs by using active feedback control over the translational velocity of two shearing surfaces to greatly extend observation times in shear flow while maintaining a constant shear rate (Figures 1 and 2). In brief, the device consists of two quartz microscope slides acting as the planar shearing surfaces affixed to two feedback-controlled motorized stages (ThorLabs). The shearing surfaces are made hydrophilic prior to sample loading in the device. Translating motors reside on top of a custom-machined aluminum bath with a glass window to provide optical access for microscopic imaging. In particular, a microscope coverslip serves as the optical window, and the coverslip−aluminum contact surface is sealed to prevent fluid leakage from the bottom of

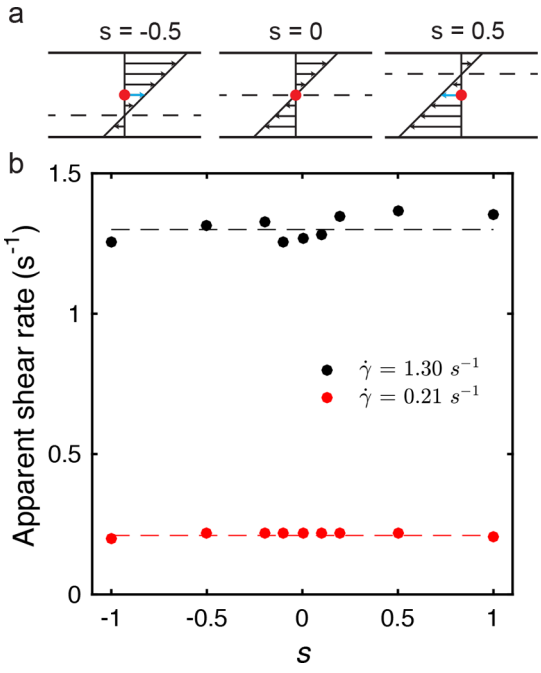

Figure 2. Feedback control for extended observation times in steady shear flow. (a) Schematic of translational velocity manipulations of shearing surfaces to maintain single polymers in the microscope field of view under constant shear rates $\dot{\gamma}$ for long observation times. Dashed lines represent the stagnation plane position. Blue arrow indicates nonzero translational velocity imparted to molecule of interest. (b) Shear rates experimentally determined by particle tracking velocimetry (data points) as a function of stagnation plane position s for two different imposed shear rates. Dashed lines show the nominal applied shear rates $\dot{\gamma}$ = 0.21 and 1.30 s^{-1} calculated from the gap thickness h and shearing wall velocities.

the bath. Prior to experiments, a polymer solution sample containing fluorescently labeled DNA in a sucrose buffer (≈3 mL) is loaded into the bath, and the two quartz microscope slides are immersed into the

https://dx.doi.org/10.1021/acs.macromol.0c01362
Macromolecules 2020, 53, 9406−9419

fluid. One of the quartz microscope slides contains a single layer of PTFE adhesive, which serves a thin spacer (thickness h = 106 μm) between the two shearing surfaces. A horizontal spring force is applied to the microscope slides to maintain a constant gap width h = 106 μm throughout the experiments. A layer of mineral oil is deposited on top of the aqueous DNA solution, thereby minimizing evaporation and maintaining a constant solution viscosity and refractive index throughout the experiments.

Prior to imaging, the shear flow apparatus is mounted on the stage of an inverted microscope (Olympus IX-81). The translating motors are connected to a computer, and the translational velocities v of the shearing walls are controlled by LabView, which enables precise application of shear rates $\dot{\gamma} = 2v/h$. The applied shear rates were verified by using particle tracking velocimetry (Figure 1d,e and Figure S1). Under these conditions, the Reynolds number $Re = \rho vh/\eta$ is sufficiently small ($Re \approx 10^{-4}$ at the highest shear rate studied), where ρ and η are the solution density and viscosity, such that inertial effects are neglected. During experiments, individual polymer molecules were imaged at least 200 μm above the surface of the coverslip viewing window to access the fully developed shear flow region (Figure S2). To increase the residence time t_{res} of a single polymer in the field of view (and hence increase the total fluid strain $\gamma = \dot{\gamma}t_{res}$), the translational velocities of the two motors were slightly varied to move the stagnation shear plane in the vicinity of the polymer while maintaining a constant velocity gradient and hence a constant shear rate $\dot{\gamma}$ (see below). In this manner, single polymer molecules are manipulated to stay within the field of view while being subjected to a constant shear rate $\dot{\gamma}$ for large fluid strains γ (up to γ = 450). In this work, we study ring polymer dynamics in steady shear flow, focusing on dynamics after transient start-up effects have ended. In this way, data are obtained and analyzed only after $\gamma \approx 70$ units of fluid strain, consistent with prior work.[34,50]

Feedback Control for Extended Observation Times in Shear Flow. Single DNA molecules are studied near the stagnation plane (y = 0) of shear flow to minimize their center-of-mass translational velocities while being subjected to finite shear rates $\dot{\gamma}$ (Figure 2). Deviations in the polymer center-of-mass away from the stagnation plane will cause the molecule of interest to eventually translate out of the field of view of the microscope. To maintain a single polymer chain within the field of view for extended observation times, the translational velocities of the shearing walls are manipulated to impart a "corrective" center-of-mass translational velocity while maintaining a constant shear rate $\dot{\gamma}$. By actively controlling the shearing wall velocities, we precisely moved the position of the stagnation plane along the gradient direction, thereby enabling single polymers to be viewed in the microscope field of view for long times. The stagnation plane position is characterized using a dimensionless parameter s:

$$s = \frac{v_1 + v_2}{v} \tag{1}$$

where v_1 and v_2 are the velocities of the top and bottom shearing wall, respectively, and v is the set point velocity used for the desired shear rate. For s = 0, $v_1 = -v_2 = v$, and the stagnation plane position is at the midpoint of the gap. As s approaches −1 or 1, the position of the stagnation plane moves toward the top or bottom shearing surface, respectively, and the molecule of interest is forced to translate left or right in the flow direction within the field of view. Importantly, a constant shear rate is maintained by the relation $v_1 - v_2 = 2v$ at all time points during the velocity manipulations (Figure 2a). As proof of principle, we validated this approach by varying the position of the stagnation plane while experimentally determining shear rates using particle tracking velocimetry (PTV) over a range of shear rates (Figure 2b). Our results show that the shear rate $\dot{\gamma}$ remains constant while the location of the stagnation plane is changed across the gap thickness. For this work, the stagnation plane was translated over relatively small distances ($-0.2 \le s \le 0.2$) by choosing molecules near the midplane of the gap within the device.

Fluorescence Microscopy and Imaging. Fluorescence imaging was performed by using an electron-multiplying charged-coupled device camera (EMCCD, Andor iXon Ultra 897) mounted on an inverted microscope (Olympus IX-81). Epi-illumination within the gap between the two shearing walls was achieved by using a 488 nm continuous wave (CW) laser (Coherent Sapphire 488 nm LP) passing through a 488 nm dichroic filter (Semrock) and a 525/50 nm bandpass emission filter (Semrock). A 1.1 NA 60× long-working distance microscope objective (Olympus) was used to image far above the coverslip window to access the fully developed shear region (Figure S2). Images were further magnified by 1.6× on the microscope, resulting in a pixel size of 0.17 μm. The acquisition time was 100 ms per frame.

Single Molecule Image Analysis. Prior to data acquisition, DNA molecules were visually inspected by stretching in flow to ensure the expected (stretched) polymer contour length (L_c = 24.9 μm for fluorescently labeled K16 circular DNA and L = 21 μm for linear λ-DNA). A custom MATLAB code was used to analyze the images by using previously reported algorithms.[47,61,62] The distribution of fluorescence intensity across multiple pixels corresponding to DNA molecules was used to determine molecular conformation parameters. The fractional chain extension stretch x/L is the extension of the molecule in the flow direction x normalized by the polymer contour length L. 2D radius of gyration tensor elements G_{ij} were calculated by using the intensity distribution of DNA in each frame:

$$G_{ij} = \sum_{m,n} \frac{I(m, n) r_i^{(m,n)} r_j^{(m,n)}}{I(m, n)} \tag{2}$$

where $I(m,n)$ is the intensity of a pixel located at the mth row and nth column, and $r_i^{m,n}$ is the distance along the ith direction for the same pixel from the center of mass of the polymer. Taking the 1-direction as the flow direction and the 2-direction as the gradient direction, the orientation angle in the flow-gradient plane is defined by using the eigenvector associated with the largest eigenvalue of the radius of gyration tensor with respect to the 1-direction:

$$\theta = \frac{1}{2} \arctan\left(\frac{2G_{12}}{G_{11} - G_{22}}\right) \tag{3}$$

With this definition, positive orientation angles correspond to the first quadrant of the flow-gradient plane, defined by the axes formed by the stagnation line and gradient axis in Figure 1c. By use of this approach, observation of polymer chain dynamics in the flow-gradient plane enables direct visualization of polymer stretch, orientation angle, and identification of polymer chain tumbling behavior.[30,63−65]

Polymer Relaxation Time and Flow Strength. The shear flow strength is defined in terms of a dimensionless group known as the Weissenberg number, $Wi = \dot{\gamma}\tau$, where τ is the longest polymer relaxation time. The polymer relaxation time τ is determined by tracking the maximum projected contour of a ring polymer (or the end-to-end extension of a linear polymer) in the flow-gradient plane following cessation of flow. In particular, the longest polymer relaxation time τ is determined by tracking fractional polymer extension in the linear entropic regime (x/L < 0.3) during chain relaxation. A single-exponential decay function is fit to the expression $(x/L)^2 = A \exp(-t/\tau) + B$, where A and B are numerical constants, as previously described.[47] In this way, τ is determined to be the ensemble average over 34 and 41 trajectories for the linear and ring DNA, respectively, yielding τ = 23.2 ± 1.2 s for linear λ-DNA and τ_c = 29.6 ± 1.5 s for K16 circular DNA. These relaxation times are consistent with prior work on ring polymer relaxation in dilute solution (Figure S3).[45,46]

Brownian Dynamics Simulations. Brownian dynamics (BD) simulations are performed on coarse-grained bead−spring chains to understand the dynamics of ring polymers in dilute solution shear flow. Details of the general BD algorithm can be found in prior work,[51,66] though here we briefly comment on extending the algorithm to ring polymers. Polymer chains are modeled as a series of N beads serving as hydrodynamic drag points connected by entropic springs. The equation of motion for each bead i is described

https://dx.doi.org/10.1021/acs.macromol.0c01362
Macromolecules 2020, 53, 9406−9419

by using an overdamped Langevin equation where inertial effects are negligible:

$$m_i\dot{\mathbf{v}}_i = \mathbf{F}_i^{\mathrm{B}} + \mathbf{F}_i^{\mathrm{d}} + \mathbf{F}_i^{\mathrm{s}} + \mathbf{F}_i^{\mathrm{EV}} \simeq 0 \tag{4}$$

where m is the mass of the ith bead, $\mathbf{F}_i^{\mathrm{B}}$ is the random thermal (Brownian) force, $\mathbf{F}_i^{\mathrm{d}}$ is the hydrodynamic drag force, $\mathbf{F}_i^{\mathrm{s}}$ is the net spring force, and $\mathbf{F}_i^{\mathrm{EV}}$ is the net interparticle excluded volume (EV) interaction forces on bead i. This equation can be manipulated to yield a set of stochastic differential equations for each bead:

$$\mathrm{d}\mathbf{r}_i = \left(\boldsymbol{\kappa}\cdot\mathbf{r}_i + \sum_{j=1}^{N}\frac{\partial}{\partial\mathbf{r}_j}\cdot\mathbf{D}_{ij} + \sum_{j=1}^{N}\frac{\mathbf{D}_{ij}\cdot\mathbf{F}_j}{kT}\right)\mathrm{d}t + \sqrt{2}\sum_{j=1}^{i}\boldsymbol{\alpha}_{ij}\cdot\mathrm{d}\mathbf{W}_j \tag{5}$$

where $\mathbf{r}_i$ denotes the position of bead i, $\mathbf{D}_{ij}$ is the diffusion tensor, $\mathbf{F}_i$ is the net interparticle force on bead i, $\mathrm{d}\mathbf{W}_i$ is representative of a Wiener process described as the product of the square root of the time step $\sqrt{\mathrm{d}t}$ with a random Gaussian vector $\mathbf{n}_i$ with zero-mean and unit variance,[67] and $\boldsymbol{\kappa}$ is the velocity gradient tensor defined for simple shear flow as

$$\boldsymbol{\kappa} = \begin{pmatrix} 0 & \dot{\gamma} & 0 \\ 0 & 0 & 0 \\ 0 & 0 & 0 \end{pmatrix} \tag{6}$$

where $\dot{\gamma}$ is the shear rate. The tensor $\mathbf{D}_{ij}$ is chosen to be the Rotne–Prager–Yamakawa (RPY) tensor, which has been shown to be positive-semidefinite for all polymer chain configurations[68] and is related to the coefficient tensor $\boldsymbol{\alpha}_{ij}$ by

$$\mathbf{D}_{ij} = \sum_{l=1}^{N}\boldsymbol{\alpha}_{il}\cdot\boldsymbol{\alpha}_{jl} \tag{7}$$

The RPY tensor is given by

$$\mathbf{D}_{ij} = \frac{kT}{\zeta}\mathbf{I}_{ij} \quad \text{if } i = j \tag{8}$$

$$\mathbf{D}_{ij} = \frac{kT}{8\pi\eta r_{ij}}\left[\left(1 + \frac{2a^2}{3r_{ij}^{\,2}}\right)\mathbf{I}_{ij} + \left(1 - \frac{2a^2}{r_{ij}^{\,2}}\frac{\mathbf{r}_{ij}\mathbf{r}_{ij}}{r_{ij}^{\,2}}\right)\right] \quad \text{if } i \neq j \text{ and } r_{ij} \geq 2a \tag{9}$$

$$\mathbf{D}_{ij} = \frac{kT}{\zeta}\left[\left(1 - \frac{9r_{ij}}{32a}\right)\mathbf{I}_{ij} + \frac{3\mathbf{r}_{ij}\mathbf{r}_{ij}}{32ar_{ij}}\right] \quad \text{if } i \neq j \text{ and } r_{ij} < 2a \tag{10}$$

where a is the bead radius, $\mathbf{r}_{ij}$ is the vector between beads i and j, ζ is the bead drag coefficient, and $r_{ij} = |\mathbf{r}_{ij}|$.

Equation 5 is nondimensionalized by using the characteristic time scale $t_s = \zeta/4H_s$, which is the relaxation time of a Hookean dumbbell, where H_s is the entropic spring constant given by $H_s = 3kT/N_{k,s}b_k^{\,2}$. Here, $N_{k,s}$ is the number of Kuhn steps per spring, b_k is the Kuhn step size, and kT is the thermal energy. The characteristic length scale $l_s = \sqrt{kT/H_s}$ corresponds to the average equilibrium length of a Hookean dumbbell, and the characteristic force scale is $F_s = \sqrt{kTH_s}$. The hydrodynamic interaction parameter h^* is defined as

$$h^* = a\sqrt{\frac{H_s}{\pi kT}} \tag{11}$$

Linear Polymers. For linear polymers, eq 5 is recast by using spring connector vectors $\mathbf{Q}_i$ for the ith spring, where $\mathbf{Q}_i = \mathbf{r}_{i+1} - \mathbf{r}_i$ such that $1 \leq i \leq N_s$, and the number of springs is $N_s = N - 1$, where N is the number of beads. In this way, the dimensionless equations of motion for the springs are written as

$$\mathrm{d}\mathbf{Q}_i = \left[Pe(\boldsymbol{\kappa}\cdot\mathbf{Q}_i) + \sum_{j=1}^{N}(\mathbf{D}_{i+1,j} - \mathbf{D}_{i,j})(\mathbf{F}_j^{\mathrm{E}} + \mathbf{F}_j^{\mathrm{EV}})\right]\mathrm{d}t + \sqrt{2}\sum_{j=1}^{i+1}(\boldsymbol{\alpha}_{i+1,j} - \boldsymbol{\alpha}_{i,j})\cdot\mathrm{d}\mathbf{W}_j \tag{12}$$

where the bead Péclet number is defined as $Pe = \dot{\gamma}\zeta/4H_s$, $\mathbf{F}_j^{\mathrm{EV}}$ is the excluded volume force exerted on bead j, and $\mathbf{F}_j^{\mathrm{E}}$ is the total entropic spring force exerted on bead j given by

$$\mathbf{F}_j^{\mathrm{E}} = \begin{cases} \mathbf{F}_1^{\mathrm{s}} & \text{if } j = 1 \\ \mathbf{F}_j^{\mathrm{s}} - \mathbf{F}_{j-1}^{\mathrm{s}} & \text{if } 1 < j < N \\ -\mathbf{F}_{N_s}^{\mathrm{s}} & \text{if } j = N \end{cases} \tag{13}$$

where $\mathbf{F}_i^{\mathrm{s}}$ is the entropic spring force on spring i. We use the Marko–Siggia spring force to model the entropic force between two adjacent beads, as this force relation has been shown to be appropriate for double-stranded DNA:[58]

$$\mathbf{F}_i^{\mathrm{s}} = \frac{kT}{b_k}\left[\frac{1}{2}\frac{1}{(1 - (Q/Q_0))^2} - \frac{1}{2} + \frac{2Q}{Q_0}\right]\frac{\mathbf{Q}_i}{Q_0} \tag{14}$$

where $Q = |\mathbf{Q}_i|$ and Q_0 is the contour length of a single spring given by $Q_0 = N_{k,s}b_k$. Excluded volume (EV) interactions are modeled by using the following energy potential:

$$U_{ij}^{\mathrm{EV}} = \frac{1}{2}\nu kTN_{k,s}^{\,2}\left(\frac{3}{4\pi R_{g,sub}^{\,2}}\right)^{3/2}\exp\left[-\frac{3r_{ij}^{\,2}}{4R_{g,sub}^{\,2}}\right] \tag{15}$$

where U_{ij}^{EV} is the EV potential between beads i and j, ν is the EV parameter, $R_{g,sub} = \sqrt{(N_{k,s}b_k)^2/6}$ is the radius of gyration of a subsection of the polymer chain, and $r_{ij} = |\mathbf{r}_{ij}|$. By use of these relations, the dimensionless EV force $\mathbf{F}_i^{\mathrm{EV}}$ on bead i in eq 12 is given by

$$\mathbf{F}_i^{\mathrm{EV}} = -\sum_{j=1;i\neq j}^{N} z\frac{9\sqrt{3}}{2}\exp\left[-\frac{3r_{ij}^{\,2}}{2}\right]\mathbf{r}_{ij} \tag{16}$$

where $z = (1/2\pi)^{3/2}\nu\tilde{N}_{k,s}^{\,2}$ and is a perturbation parameter for EV interactions in analytic theories.[67,69] The stochastic differential equations given by eq 12 are solved by using an efficient second-order predictor–corrector algorithm as previously described.[32] Prior to the initiation of flow, the polymer chains were allowed to equilibrate for at least 10τ to ensure random initial polymer conformations.

Ring Polymers. For ring polymers, the number of springs is equal to the number of beads such that $N_s = N$, and the connector vectors are defined as

$$\mathbf{Q}_i = \begin{cases} \mathbf{r}_{i+1} - \mathbf{r}_i & \text{if } 1 \leq i < N_s \\ \mathbf{r}_1 - \mathbf{r}_N & \text{if } i = N_s \end{cases} \tag{17}$$

For springs $1 \leq i < N_s$, then the equations of motion are written as

$$\mathrm{d}\mathbf{Q}_i = \left[Pe(\boldsymbol{\kappa}\cdot\mathbf{Q}_i) + \sum_{j=1}^{N}(\mathbf{D}_{i+1,j} - \mathbf{D}_{i,j})(\mathbf{F}_j^{\mathrm{E}} + \mathbf{F}_j^{\mathrm{EV}})\right]\mathrm{d}t + \sqrt{2}\sum_{j=1}^{i+1}(\boldsymbol{\alpha}_{i+1,j} - \boldsymbol{\alpha}_{i,j})\cdot\mathrm{d}\mathbf{W}_j \tag{18}$$

and for spring $i = N_s$, the equation of motion is

https://dx.doi.org/10.1021/acs.macromol.0c01362
Macromolecules 2020, 53, 9406–9419

$$d\mathbf{Q}_i = \left[Pe(\boldsymbol{\kappa}\cdot\mathbf{Q}_i) + \sum_{j=1}^{N} (\mathbf{D}_{1,j} - \mathbf{D}_{N,j})(\mathbf{F}_j^{E} + \mathbf{F}_j^{EV}) \right] dt + \sqrt{2} \sum_{j=1}^{N} (\boldsymbol{\alpha}_{1,j} - \boldsymbol{\alpha}_{N,j})\cdot d\mathbf{W}_j \quad (19)$$

where the total entropic spring force $\mathbf{F}_j^{E}$ exerted on bead j is given by

$$\mathbf{F}_j^{E} = \begin{cases} \mathbf{F}_1^{s} - \mathbf{F}_{N_s}^{s} & \text{if } j = 1 \\ \mathbf{F}_j^{s} - \mathbf{F}_{j-1}^{s} & \text{if } 1 < j < N \\ \mathbf{F}_{N_s}^{s} - \mathbf{F}_{N_s-1}^{s} & \text{if } j = N \end{cases} \quad (20)$$

The stochastic differential equations for ring connectors given by eqs 18 and 19 are solved by using a similar second-order predictor−corrector algorithm used for linear chains. Prior to the initiation of flow, the polymer chains were allowed to equilibrate for at least 10τ to ensure random initial polymer conformations.

BD Simulation Parameters. Coarse-grained BD simulations used the following parameters. For linear polymers, $N_s = 16$ and $N_{k,s} = 10$ (giving $N_k = 160$) with $h^* = 0.2$ and $\nu = 0.001\ \mu m^3$, similar to prior work.[66] We simulated two ring polymer molecular weights, $N_k = 180$ and $N_k = 380$, both with $N_{k,s} = 10$, using the same HI and EV parameters for linear chains. The molecular weight ratio of rings to linear chains $N_{k,ring}/N_{k,linear}$ for larger rings is $380/160 \simeq 2.4$, which matches the molecular weight ratio of the ring and linear DNA in experiments (114.8 kbp/48.5 kbp $\simeq$ 2.4). The polymer relaxation time τ was determined by initializing bead−spring polymers in an extended conformation (fractional extension >0.6), followed by tracking the maximum extension of the ring or linear chain during relaxation in the absence of flow. The longest relaxation times were determined by fitting the fractional extension to a single exponential $(x/L)^2 = A\exp(-t/\tau) + B$ over the range $x/L < 0.3$ or $x/L_c < 0.3$ in a similar manner to experiments.[66] This process was repeated over an ensemble of 100 molecules. For each Wi, the bead−spring polymers were simulated for 10^5 strain units.

RESULTS AND DISCUSSION

We began by observing the stretching dynamics of single ring polymers in the flow-gradient plane of shear. Following the onset of shear flow, ring polymers initially stretch from their equilibrium coiled state, rotate, and align toward the flow axis. In this work, we focus on the steady shear behavior of ring polymers, corresponding to dynamics after the initial transient start-up phase (i.e., after $\gamma \approx 70$ units of strain following the onset of flow).[30] Similar to linear polymers in dilute solution shear flow,[30,51,52] ring polymers do not adopt a steady-state conformation in steady shear flow. In fact, our results show that ring polymers undergo repeated chain stretching and tumbling events in shear.

A series of dynamic trajectories for a ring polymer in steady shear ($Wi = 6.2$) with a corresponding set of representative single molecule images are shown in Figure 3. Here, the ring polymer fractional extension x/L_c and transient orientation angle θ are plotted as a function of time and applied fluid strain γ. Single molecule snapshots in Figure 3a correspond to the labeled time points in the trajectories in Figures 3b and 3c. Sharp transitions in the orientation angle (e.g., between time points denoted by *ii* and *iii*) are typically accompanied by a corresponding local minimum in the fractional extension. This behavior corresponds to a polymer tumbling event, initiated when an aligned polymer fluctuates into a conformation with a negative orientation angle, thereby causing the polymer chain to rapidly advect with the flow and undergo a tumbling event.

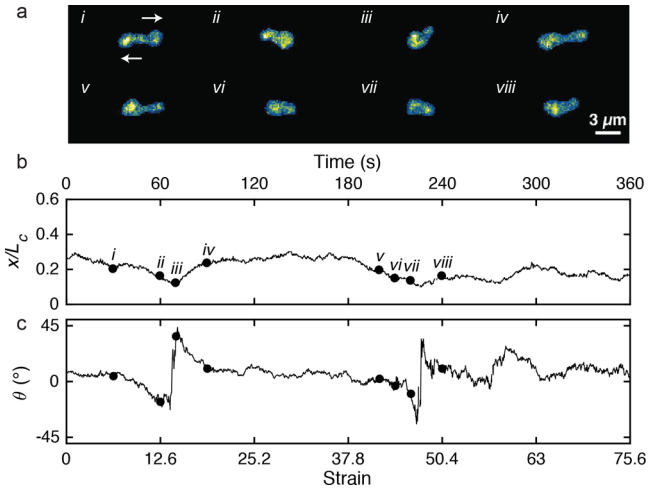

Figure 3. Characteristic single molecule images and trajectories of ring polymers in steady shear flow at $Wi = 6.2$. (a) Single molecule snapshots of K16 ring DNA undergoing two distinct tumbling events, where individual images correspond to the labeled time points in the trajectories shown below. Arrows in panel *i* indicate shear direction. (b, c) Associated trajectories of transient fractional extension x/L_c and transient orientation angle θ for a ring polymer in steady shear.

In general, we observe that ring polymers open into a looped conformation in steady shear, such that ring contour "opens up" in the vorticity direction. These observations are consistent with prior simulations,[55,70] which reported vorticity-direction swelling of ring polymers in shear flow. In our experiments, the diameter of the open loop conformation of K16 circular DNA ($L_c = 24.9\ \mu m$) in flow is slightly larger than the depth of field of the microscope ($\approx 1\ \mu m$). As a result, fluorescently labeled ring polymers appear with one strand of the ring in sharp focus, with the second strand slightly out of focus in an adjacent focal plane. Nevertheless, the two strands of the stretched ring polymer can be imaged by adjusting the microscope focus over a small distance $\approx 3-5\ \mu m$ along the vorticity axis, which is perpendicular to the flow-gradient direction. Occasionally, conformational fluctuations result in the two ring strands appearing in sharp focus in the flow-gradient plane, such that the closed ring contour is clearly visible in the microscope image. Interestingly, prior work on single ring polymer dynamics in planar extensional flow revealed an analogous behavior, where the ring polymer contour "opens up" into a looped conformation along the zero-flow axis due to intramolecular hydrodynamic interactions (HI).[45,46]

A series of characteristic trajectories for transient fractional extension x/L_c are shown in Figure 4a, with corresponding simultaneous trajectories for orientation angle θ shown in Figure 4b, such that side-by-side plots correspond to the same individual ring polymer at the given Wi. Around $Wi \approx 0$, ring polymers are not significantly stretched beyond equilibrium, and polymer chain orientation is nearly isotropic with no bias toward a particular orientation angle. Above $Wi \approx 6$, ring polymers tend to align with the flow axis (toward $\theta = 0°$) as Wi increases. In general, the magnitude and frequency of fluctuations in fractional extension x/L_c increase as Wi increases. Moreover, higher flow strengths generally lead to more frequent tumbling events, as evidenced by the increase in fluctuations in θ that simultaneously occur with minima in x/L_c ($Wi = 62$, bottom panel, Figures 4a and 4b). Ring polymer

https://dx.doi.org/10.1021/acs.macromol.0c01362
Macromolecules 2020, 53, 9406−9419

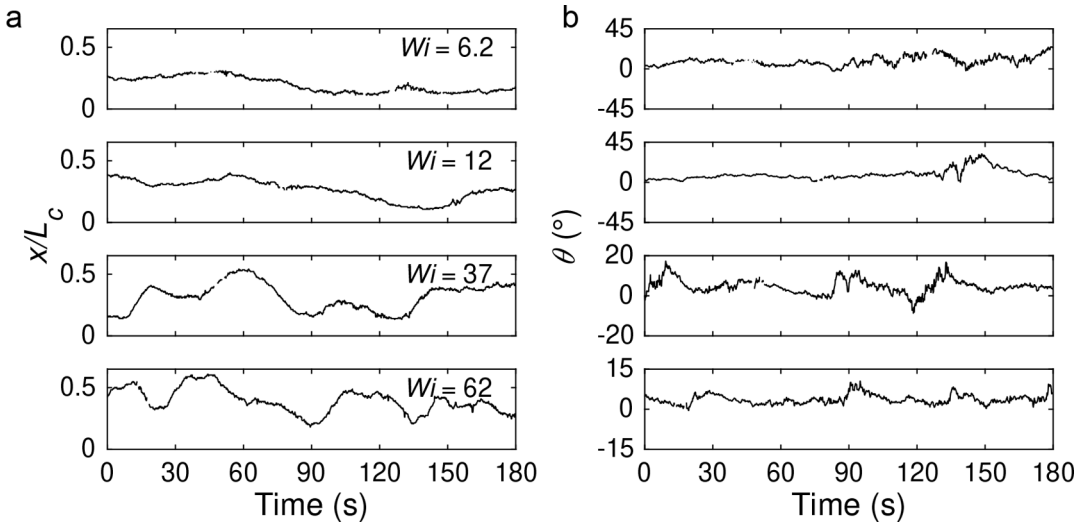

Figure 4. Representative single ring polymer trajectories in steady shear flow as a function of *Wi*. (a) Transient fractional extension of a single K16 ring DNA as a function of *Wi*. (b) Corresponding transient orientation angle trajectories for the same ring polymer at the same *Wi* shown in (a). The vertical scales are adjusted at high *Wi* for clarity.

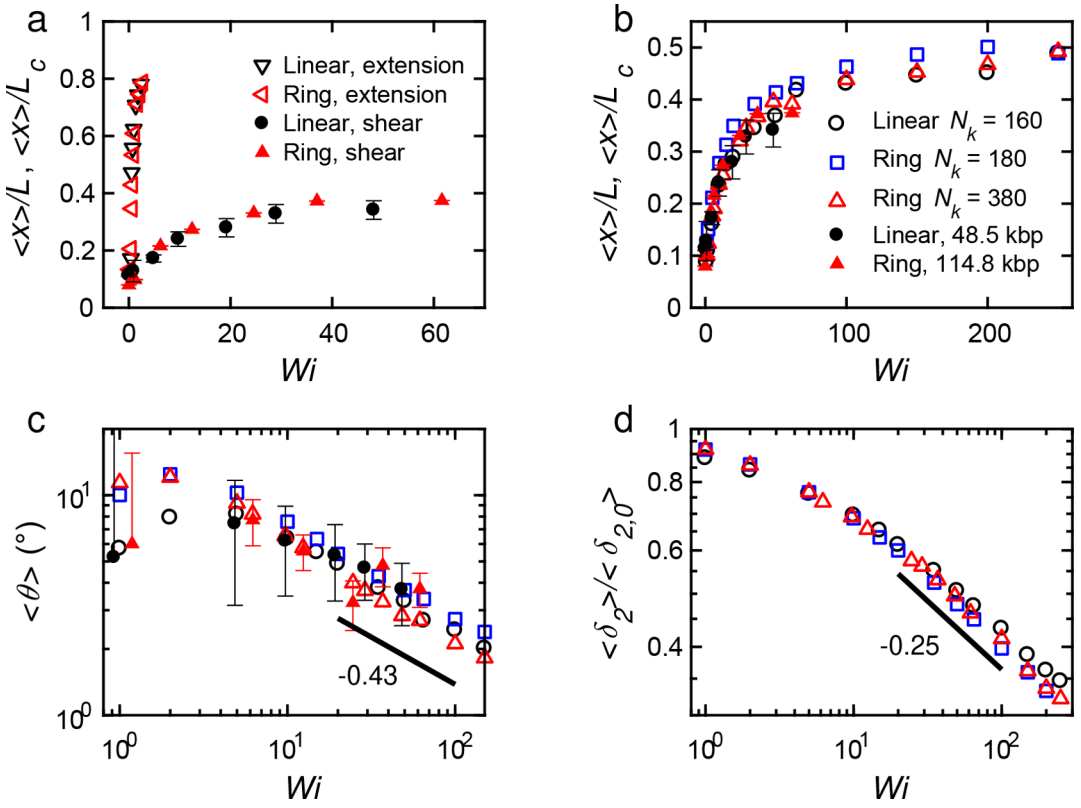

Figure 5. Ensemble-averaged fractional polymer extension, orientation angle, and gradient thickness in steady shear. (a) Effect of flow type and polymer topology on average polymer fractional extension. Ensemble-averaged fractional polymer extension is shown for rings and linear chains in shear flow and planar extensional flow, with the latter taken from prior work.[45] All data shown in (a) are obtained from single molecule experiments. (b) Ensemble-averaged fractional extension $\langle x\rangle/L$ or $\langle x\rangle/L_c$, (c) orientation angle $\langle\theta\rangle$, and (d) scaled gradient thickness $\langle\delta_2\rangle/\langle\delta_{2,0}\rangle$ as a function of *Wi* from experiments (closed symbols) and simulations (open symbols), where $\langle\delta_{2,0}\rangle$ is the gradient-direction thickness at $Wi = 0$.

tumbling is quantified by using cross-correlation analysis, as discussed below.

Ensemble average fractional extension $\langle x\rangle/L_c$, orientation angle $\langle\theta\rangle$, and dimensionless gradient thickness $\langle\delta_2\rangle/\langle\delta_{2,0}\rangle$ for ring polymers in steady shear are shown in Figure 5 as a function of *Wi* from both single molecule experiments and BD simulations. Figure 5a shows a comparison of the average fractional polymer extension for rings and linear DNA in shear flow and planar extensional flow from experiments, where ring stretching data in extensional flow are taken from prior single molecule experiments.[45] In extensional flow, linear and ring polymers attain high degrees of extension (x/L or $x/L_c > 0.7$) at relatively low *Wi* ($Wi \leq 2$). In contrast, linear and ring polymers generally show much smaller degrees of average

https://dx.doi.org/10.1021/acs.macromol.0c01362
Macromolecules 2020, 53, 9406−9419

fractional extension in steady shear flow across a wide range of Wi ($6.2 \leq Wi \leq 62$). These results are consistent with prior single molecule studies of linear chains in steady shear showing that the average fractional extension asymptotes to $x/L \approx 0.5$ at high Wi due to the rotational component of shear flow.[29,51]

In general, we observe no quantitative differences in the average fractional extension of ring polymers compared to their linear analogues in shear. In contrast, a shifted coil−stretch transition in planar extensional flow was observed for ring polymers compared to linear chains due to hydrodynamic backflow effects.[45,46] In extensional flow, rings adopt highly stretched conformations wherein the two strands of the ring approach in close proximity, resulting in intramolecular hydrodynamic coupling effects.[46] In shear flow, however, rings are stretched to smaller degrees of extension and do not regularly adopt the (steady) highly stretched conformations observed in extensional flow. Indeed, transient stretching trajectories for $Wi \leq 62$ (Figure 4) show that rings rarely stretch to fractional extensions $x/L_c \geq 0.5$, where the hydrodynamic coupling effects were observed to have a significant impact in extensional flow.[46] Moreover, ring polymers exhibit highly dynamic conformations in shear, evidenced by repeated tumbling events in flow. We posit that the dynamical nature of this process (in part) precludes the formation of stable open loop conformations of rings in the flow-gradient plane of shear. However, our results support the notion of an open loop ring conformation in the flow-vorticity plane, which is consistent with recent simulations of ring polymers in shear flow.[55,70]

The average fractional extension of ring and linear polymers is shown in Figure 5b from experiments and BD simulations. The experimental data on linear chains are in good agreement with prior work on linear DNA in shear flow (Figure S4a).[29,30] Moreover, experimental data are in good agreement with results from BD simulations for both rings ($N_k = 380$) and linear chains ($N_k = 160$). A slight increase in the average fractional extension is observed from BD simulations of smaller molecular weight rings with $N_k = 180$, which may arise due to an approach to universal behavior as molecular weight increases. Figure 5c shows the average orientation angle $\langle\theta\rangle$ plotted as a function of Wi for linear and ring polymers. As Wi increases, the average orientation angle decreases as the polymer chains spend more time aligned with the flow axis. Our experimental results show that the average orientation angles for ring and linear polymers follow a similar power-law relation with Wi at low to intermediate Wi values, such that $\langle\theta\rangle \propto Wi^{-0.30}$ over the range $5 \leq Wi \leq 62$ (Figure S4b). At higher Wi, the BD simulation results for $Wi > 50$ reveal a steeper power-law dependence of $\langle\theta\rangle \propto Wi^{-0.43}$. Prior single molecule experiments and simulations[30,51] of linear polymers in shear flow reported a similar dependence of average orientation angle on flow strength, such that $\langle\theta\rangle \propto Wi^{-0.43}$, where these prior studies focused on polymer chain dynamics at higher Wi values ($5 \leq Wi \leq 600$ in experiments[30] and $10 \leq Wi \leq 1000$ in simulations[51]).

The polymer gradient-direction thickness δ_2 is directly related to macroscopic properties such as shear viscosity[30,51] and is defined as $\delta_2 = \sqrt{G_{22}}$. In Figure 5d, ensemble-averaged gradient-direction thickness $\langle\delta_2\rangle$ is plotted from BD simulations while normalized by the value at equilibrium $\langle\delta_{2,0}\rangle$. Results from BD simulations show that the normalized values of $\langle\delta_2\rangle/\langle\delta_{2,0}\rangle$ show similar power-law scaling behavior as a function of Wi, such that $\langle\delta_2\rangle/\langle\delta_{2,0}\rangle \propto Wi^{-0.27}$ for ring polymers with $N_k = 380$, $\langle\delta_2\rangle/\langle\delta_{2,0}\rangle \propto Wi^{-0.29}$ for rings with $N_k = 180$, and $\langle\delta_2\rangle/\langle\delta_{2,0}\rangle \propto Wi^{-0.24}$ for linear chains with $N_k = 160$ over the range $60 \leq Wi \leq 250$. Moreover, these scaling behaviors are in good agreement with prior BD simulations of linear chains, where $\langle\delta_2\rangle/\langle\delta_{2,0}\rangle \propto Wi^{-0.26}$ and single polymer experiments on $L = 84$ μm DNA $\langle\delta_2\rangle/\langle\delta_{2,0}\rangle \propto Wi^{-0.27}$.[51] In the prior experiments and BD simulations, the range of Wi studied extends up to $Wi = 10^3$ in simulations and $Wi = 584$ for experiments. In our experiments, we were unable to accurately quantify δ_2 values for ring DNA due to unavoidable ring chain fluctuations, which unlike linear chains results in significant fluorescence intensity fluctuations and uncertainties due to the adjacent, out-of-focus strand for ring DNA.

Ensemble-averaged real-space polymer chain conformations in steady shear are shown in Figure 6. Here, individual polymer snapshots from experiments are superimposed by summing the fluorescence intensity at each pixel relative to the polymer center of mass at each frame. The resultant images are shown in Figure 6, where conformational maps of ring and linear polymers are shown as a function of Wi. As Wi increases, the conformations shift away from an isotropic distribution to a highly anisotropic distribution, denoting polymer stretching and alignment in shear flow. These observations are generally consistent with the decrease in average orientation angle $\langle\theta\rangle$ as Wi increases.

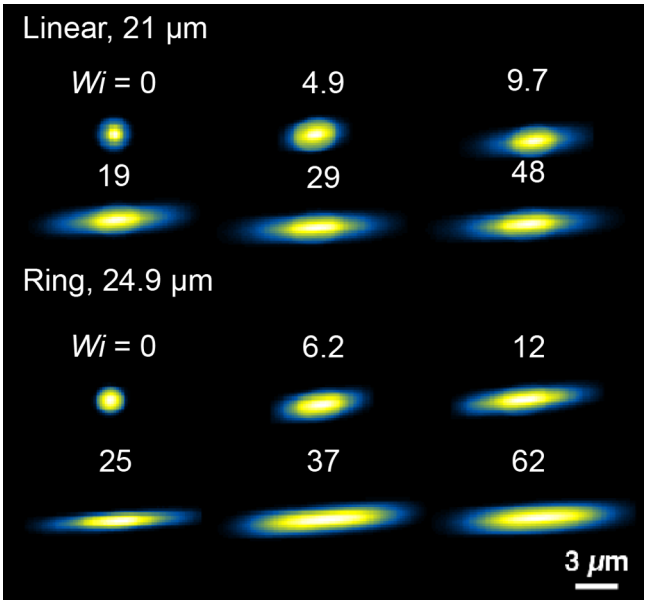

Figure 6. Temporally averaged real-space conformational maps of DNA in shear as a function of Wi. Image are generated by averaging all fluorescence intensity distributions relative to the intensity-weighted polymer center of mass over all frames for each Wi. False color is applied to the normalized grayscale images.

We next determined the distributions in fractional extension and orientation angle for linear chains and rings (Figures 7 and 8). Probability distributions of fractional chain extension for linear chains and rings in steady shear are shown in Figure 7. Although linear chains and rings show nearly equal average fractional polymer extension as a function of Wi (Figure 5), the distributions of fractional polymer extension are qualitatively different for these polymer architectures in steady shear. Linear polymers show very broad distributions that tail toward larger

https://dx.doi.org/10.1021/acs.macromol.0c01362
Macromolecules 2020, 53, 9406−9419

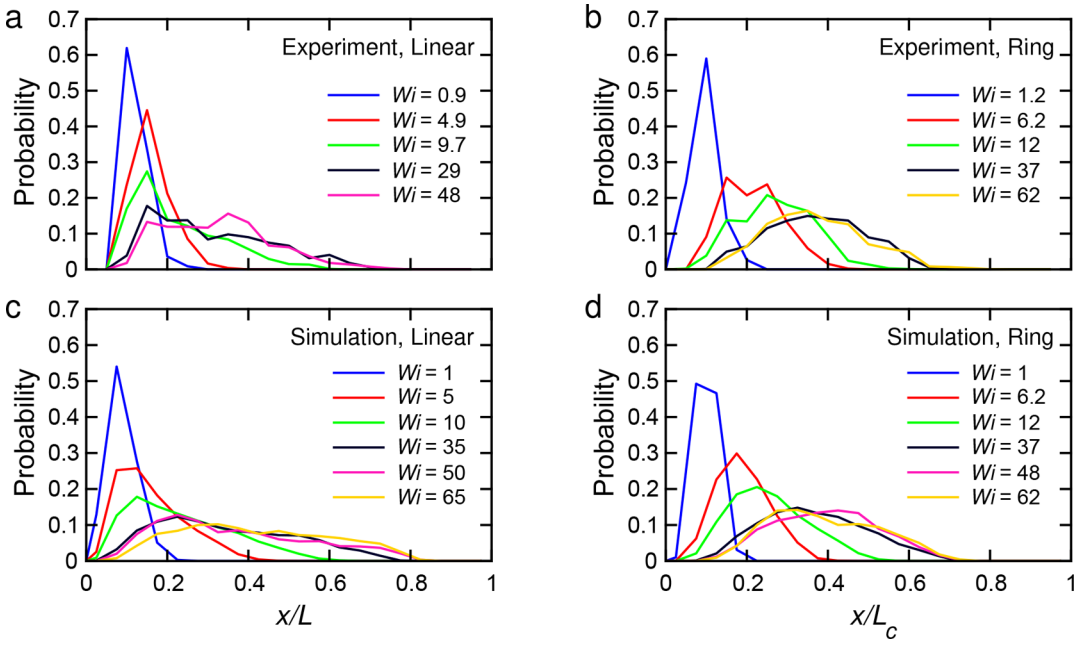

Figure 7. Probability distributions of fractional extension for rings and linear chains in steady shear flow. (a, b) Probability distributions of fractional extension from single molecule experiments of 48.5 kbp linear DNA and 114.8 kbp ring DNA, respectively, as a function of *Wi*. Bin sizes are 0.05. Each ensemble is based on ~10^4 individual molecular images. (c, d) Probability distributions of fractional extension from BD simulations of N_k = 160 linear chains and N_k = 380 ring chains, respectively, as a function of *Wi*.

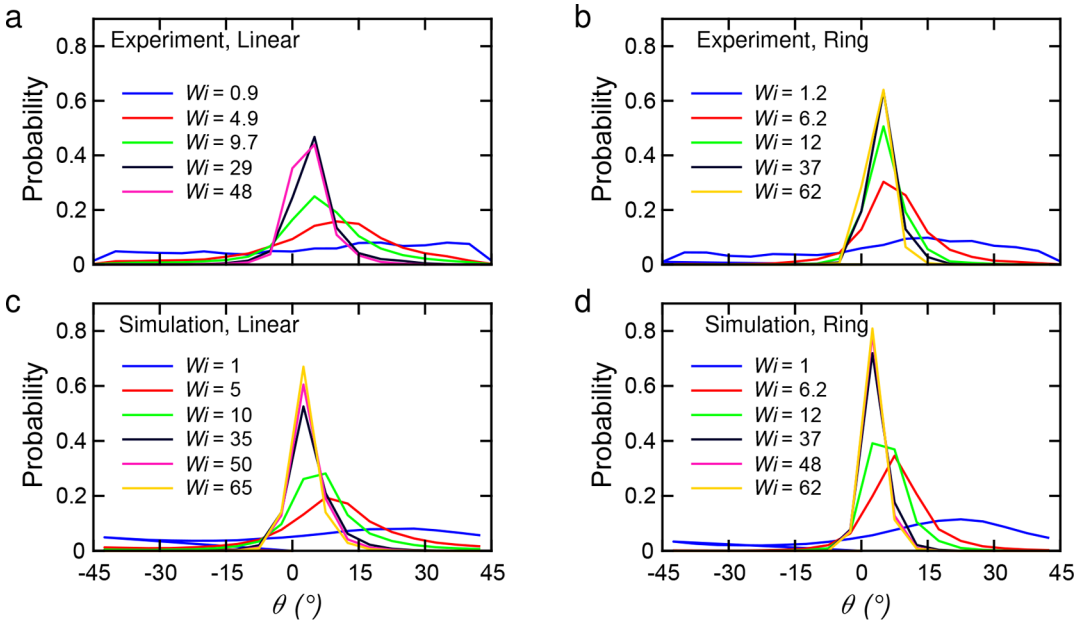

Figure 8. Probability distributions of orientation angle θ for rings and linear chains in steady shear flow. (a, b) Probability distribution of orientation angle from single molecule experiments of 48.5 kbp linear DNA and 114.8 kbp ring DNA, respectively, as a function of *Wi*. (c, d) Probability distribution of orientation angle from BD simulations of N_k = 160 linear chains and N_k = 380 rings, respectively, as a function of *Wi*. Bin sizes are 5°.

chain extensions (Figures 7a and 7c), which generally agrees with previous single molecule studies of linear chains in shear flow.[30,52] On the other hand, the distributions of fractional extension for rings are nearly symmetric at higher flow strengths $Wi \geq 30$ (Figures 7b and 7d). These differences are observed in both experiments and BD simulations. We also observe these differences in BD simulations of rings and linear chains with similar total molecular weights (Figure S5), corresponding to BD simulations of rings with N_k = 180. Indeed, such qualitative differences in molecular conformation are also reflected in the average real-space chain conformations shown in Figure 6, where regions of higher intensities are more localized near the center of mass for linear polymers, corresponding to larger probabilities of chain distribution at smaller fractional extensions ($x/L \approx 0.2$) over the range of *Wi* in this work. As previously discussed, the fully stretched contour length of the K16 ring DNA (L_c = 24.9 μm) is slightly larger than the contour length of linear DNA (L = 21 μm)

https://dx.doi.org/10.1021/acs.macromol.0c01362
Macromolecules 2020, 53, 9406−9419

used in this work; however, we do not expect such small differences in molecular weight to give rise to qualitatively different probability distributions in chain extension shown in Figure 7. Prior single molecule experiments on polymer stretching in extensional flow also examined linear and ring DNA molecules with similar, small differences in molecular weight,[45] and it was shown that the shifted coil−stretch transition for rings was independent of molecular weight and only a consequence of topology. We posit that differences in the probability distributions of chain extension similarly arise due to differences in chain architecture and not due to small differences in molecular weight.

Probability distributions of orientation angles are shown in Figure 8 for linear and ring polymers from both experiments and simulations. Interestingly, θ distributions show qualitatively similar shapes for rings and linear chains in steady shear, despite differences in the probability distributions of fractional extension. However, both experiments and BD simulations show that ring polymers exhibit a sharper peak at higher Wi ($Wi \gtrsim 30$) when compared to their linear counterparts. This may be another consequence of the ring topology conferring less conformational degrees of freedom in shear flow, leading to narrower distributions. Overall, orientation angle distributions show that (on average) both ring and linear polymers adopt more highly aligned conformations at larger *Wi*, indicated by the peaks in the distributions approaching $\theta = 0°$ for increasing *Wi*. Moreover, polymer chain advection plays an increasingly dominant role at higher *Wi* compared to thermal fluctuations, leading to rapid chain alignment and reorientation events and resulting in an overall narrowing of the orientation angle distributions as *Wi* increases.

Our results provide clear evidence for ring polymer tumbling motion in shear flow (Figure 3 and Movie S1). Tumbling phenomena have been previously observed for linear polymer chains in shear flow.[30,52] The mechanism is generally understood to follow a characteristic sequence of events, starting with polymer stretching along the extensional axis of shear flow, followed by alignment toward the flow axis due to the rotational component of shear flow and the finite extensibility of polymer chains, and concluding with a Brownian fluctuation inducing a negative orientation angle. As a result, the polymer chain adopts an unfavorable conformation with respect to the flow axis, resulting in a rapid end-over-end tumbling event.[52] Although ring polymers have no free ends, our results show that rings stretch and align along the flow axis, occasionally experiencing a thermal fluctuation that drives the polymer chain into a negative orientation angle, thereby giving rise to a tumbling event. Our results show that (as expected) this process is not deterministic, such that a ring polymer does not necessarily tumble after aligning with the flow axis. Rather, Brownian fluctuations may instead rotate the polymer toward a more positive orientation angle (away from the flow axis), followed by a subsequent "restretching" event in flow. Restretching events following stretching and alignment in steady shear have been similarly observed for linear polymers.[30,52]

To quantify the tumbling dynamics of ring polymers in shear flow, we determined cross-correlations of fractional extension x/L and gradient thickness δ_2. The normalized cross-correlation function is defined as[51]

$$C_{x/L,\delta_2}(T) = \frac{\langle (x/L)'(t)\delta_2'(t+T)\rangle}{\sqrt{\langle (x/L)'^2\rangle\langle \delta_2'^2\rangle}} \quad (21)$$

where the primes indicate quantities relative to their average (mean) values. Figure 9a shows cross-correlations from BD simulations of linear and ring chains at two different flow strengths. For all *Wi*, cross-correlations show a peak corresponding to positive correlations at negative lag times and a valley corresponding to negative correlations at positive lag times. The peak at negative lag times indicates that large fractional extensions are correlated to prior large gradient thicknesses and that small fractional extensions tend to follow small δ_2 values. These behaviors correspond to polymer stretching from coiled states and polymer retraction following stretched states. The negative correlation at positive lag times indicates that large polymer extension events tend to be followed by decreasing δ_2 values due to the finite extensibility of the chain and that small fractional extensions are followed

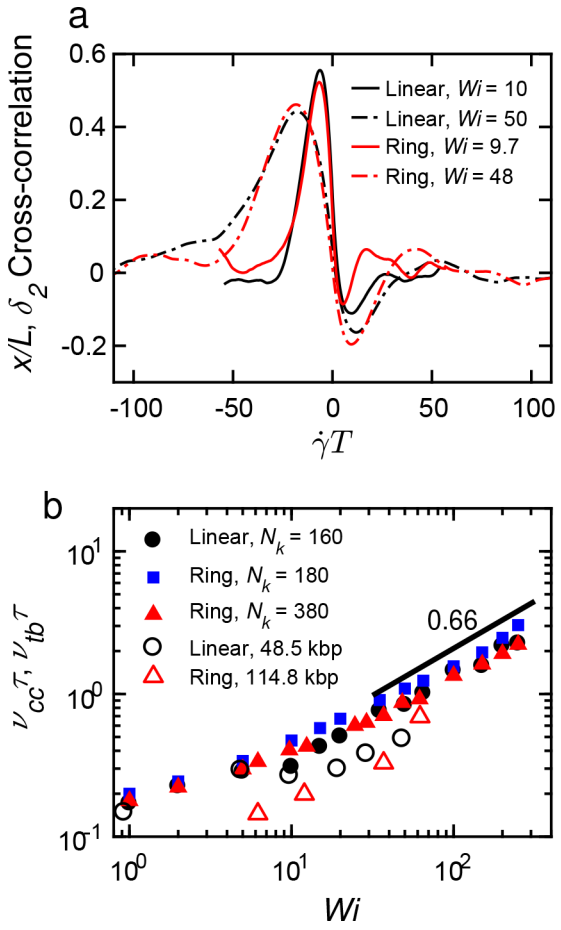

Figure 9. Cross-correlations and polymer tumbling frequency in steady shear flow. (a) Cross-correlation between x'/L and δ_2', where the primes indicate mean-subtracted quantities, from BD simulations of $N_k = 160$ linear chains (black) and $N_k = 380$ rings (red) for $Wi = 10$ (solid lines) and $Wi = 50$ (dashed lines) for the linear and ring topologies, respectively. The lag time T is nondimensionalized by the shear rate $\dot{\gamma}$. (b) Dimensionless tumbling frequencies (scaled with relaxation times) from BD simulations using the peak and valley separation time scales from cross-correlations as a function of *Wi*. Also shown is the scaled tumbling frequency from single molecule experiments of DNA trajectories.

https://dx.doi.org/10.1021/acs.macromol.0c01362
Macromolecules 2020, 53, 9406−9419

by increasing δ_2 values corresponding to polymer recoiling events. At long lag times, the cross-correlations decay to zero, indicating that any coupled motion in the flow and gradient directions is not perfectly periodic.

Tumbling frequencies are determined from the cross-correlations (ν_{cc}) by using the offset time between peaks and valleys such that $\nu_{cc} = [2(T_+ - T_-)]^{-1}$, where T_+ and T_- correspond to the valley and peak lag times of the cross-correlation at positive and negative offset times, respectively.[54,55] Figure 9b shows these polymer tumbling frequencies scaled by the polymer relaxation time as a function of *Wi*. BD simulations of linear chains and rings with $N_k = 380$ show similar tumbling frequencies over the range of *Wi* shown. BD simulations of smaller MW rings ($N_k = 180$) show slightly larger scaled tumbling frequencies compared to rings of higher molecular weight or linear chains. As a reference, we show the sublinear tumbling frequency scaling $\propto Wi^{0.66}$ for linear polymers in shear flow from prior work,[52] which appears in good agreement with our results on ring polymers. Tumbling frequencies from single molecule experiments are also shown in Figure 9b for 48.5 kbp linear and 114.8 kbp ring DNA, determined by manual counting of end-over-end tumbling events from recorded trajectories.

We further determined the power spectral density (PSD) of polymer orientation angle in shear flow. The power spectral density is the Fourier transform of the autocorrelation of a stationary stochastic signal and gives the power contribution $P(\nu)$ from a frequency ν from

$$P(\nu) = \int_{-\infty}^{\infty} C_{\theta,\theta}(T) e^{-2i\pi\nu T}\, dT \tag{22}$$

where $C_{\theta,\theta}(T) = \langle\theta(t)\theta(t+T)\rangle$. Prior work on the dynamics of linear polymers in dilute solution shear flow revealed the existence of characteristic periodic tumbling motion of polymers as determined by the presence of a peak in the PSD of orientation angle θ.[52]

Representative PSDs of orientation angle for a ring polymer in shear flow are shown in Figure 10a. A clear peak is observed for the PSD of θ of ring polymers in shear. As *Wi* increases, the peak is shifted toward higher frequencies, indicating that the characteristic periodic time scale decreases with increasing flow strength. The peak frequency from PSDs of θ (ν_{PSD}) as a function of *Wi* are plotted in Figure 10b. The peak frequency scaling with *Wi* is sublinear and appears to scale as $\nu_{PSD} \propto Wi^{0.55}$, which is a slightly smaller power-law exponent compared to the scaling of ν_{cc} determined from cross-correlations and from prior work on linear chains.[52] We attribute this difference due to the limited range of *Wi* studied in the present work; prior work on linear polymers in shear showed that $\nu_{PSD} \propto Wi^{0.66}$ for $Wi \geq 300$, whereas the present work only examines dynamic behavior up to $Wi \leq 250$. Moreover, we determined tumbling frequencies of linear DNA and ring DNA from single molecule experiments by visual inspection of end-over-end tumbling events. In general, the ring polymers studied in this work do not exhibit a clear difference from linear counterparts in terms of the peak frequency scaling behavior as a function of *Wi*.

In general, cross-correlations and PSD analyses for linear and ring polymers show similar scaling behavior as a function of flow strength. This may imply a similar general framework for the molecular-level motions that drive the dynamics in shear flow for linear and ring polymer architectures. In shear flow, our results show that ring polymers generally undergo

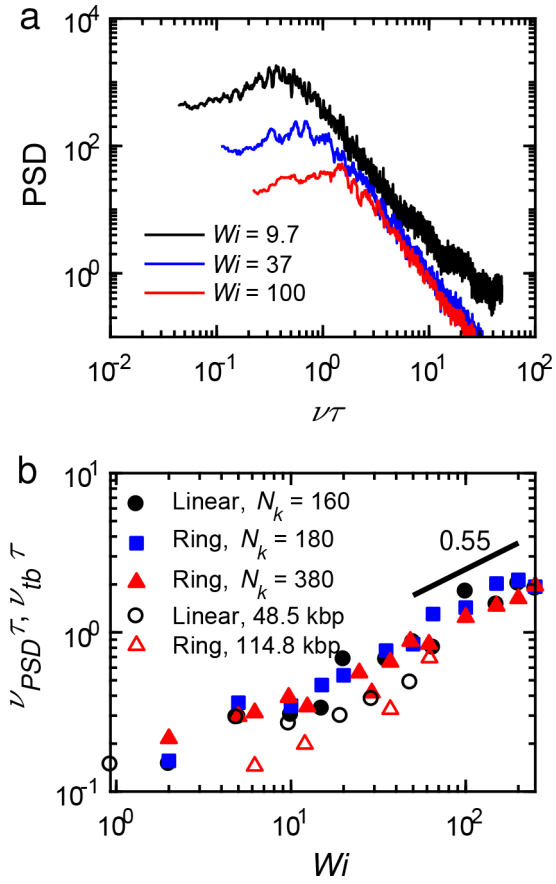

Figure 10. Power spectral density (PSD) of orientation angle and polymer tumbling frequency in steady shear flow. (a) PSDs of orientation angle θ from BD simulations of rings with $N_k = 380$ rings in shear as a function of *Wi*. The frequencies are scaled by the longest polymer relaxation time τ. (b) Peak frequencies from PSDs scaled by the longest polymer relaxation time τ as a function of *Wi*. Also plotted are tumbling frequencies of 48.5 kbp linear and 114.8 kbp ring DNA from single molecule experiments (open symbols).

cyclic (yet aperiodic) stretching, alignment, and tumbling behavior in a similar fashion to their linear counterparts.[30,51,52] However, qualitative differences are observed in the probability distributions of fractional extension between these two chain architectures, suggestive of subtle differences in the conformational tumbling dynamics in shear that may not be captured using strain-averaged quantities such as cross-correlations and power spectra. The closed contour of a ring polymer generally decreases the conformational degrees of freedom compared to linear chains. Prior work has shown that ring polymers exhibit greatly reduced diversity in molecular conformations during the transient stretching process in the start-up of extensional flow.[45] Linear polymers are known to exhibit a wide variety of transient molecular conformations when stretching from a coiled state in extensional flow, including dumbbell, half-dumbbell, kinked, and folded conformational pathways.[31] On the other hand, ring polymers primarily stretched via a continuous elongation or uniform stretching pathway in extensional flow, with a small molecular subpopulation of rings (≈7%) showing hindered stretching due to the formation of transient knots.[45,46] Our results suggest that the continuous elongation pathway exhibited by rings intrinsically avoids the dynamically slower conformational stretching pathways ex-

https://dx.doi.org/10.1021/acs.macromol.0c01362
Macromolecules 2020, 53, 9406−9419

hibited by linear chains associated with more compact chain formations.[31]

CONCLUSIONS

In this work, we study the dynamics of single ring polymers in steady shear flow using single-molecule visualization and Brownian dynamics simulations. Observation of ring polymer dynamics in the flow-gradient plane provides a direct window into characterizing orientation angle alignment and periodic chain motion driven by a coupling between gradient and flow-direction behavior.[51,52] Using this approach, we simultaneously track transient polymer extension, orientation angle, and gradient thickness in shear flow. Our results show that ring polymers undergo tumbling motion in shear, as reflected by abrupt negative to positive transitions in the orientation angle, as well as single molecule conformational images showing chain tumbling behavior. Overall, ring polymers exhibit similar average fractional extension in steady shear as a function of *Wi* compared to linear polymer analogues. Interestingly, we observe significant differences in the distributions of fractional chain extension for ring and linear polymers in shear flow, yet we do not find clear differences in flow-gradient cross correlations and power spectral densities based on the orientation angle dynamics. Such differences in underlying molecular ensembles can only be accessed using single molecule techniques, which reveal unexpected differences due to distinct molecular architectures in this work.

Our work provides a new set of single molecule observations of ring polymer dynamics in steady shear. Nevertheless, several open questions remain regarding the nonequilibrium dynamics of ring polymers in flow. Prior simulations have reported unexpected nonequilibrium ring polymer conformations at high *Wi*, including the emergence of possible nonmonotonic flow-induced conformational effects for ring polymers due to intramolecular HI.[70,71] However, the present work focuses on the steady shear dynamics of ring polymers at low to intermediate *Wi* values, which precludes observation of putative S-shaped ring polymer conformations at high *Wi*. Furthermore, our observation of flow-induced ring-opening in the vorticity direction warrants additional single molecule studies on ring polymer dynamics in the flow-vorticity plane, which would enable quantification of ring inflation in flow. In addition, it is unclear how the tumbling dynamics of rings will change at higher polymer concentrations or in the presence of linear chains in the background solution, given that ring−linear chain threading events were observed in prior single molecule studies in semidilute unentangled solutions.[47] Overall, our work opens new avenues for performing single molecule experiments on ring polymers in more complex and nondilute systems, where intermolecular interactions are expected to play a key role in determining nonequilibrium chain dynamics.

ASSOCIATED CONTENT

Supporting Information

The Supporting Information is available free of charge at https://pubs.acs.org/doi/10.1021/acs.macromol.0c01362.

Particle tracking velocimetry and shear rate determination in the flow-gradient device; flow field characterization; longest relaxation time comparison to prior single molecule measurements; comparison of average fractional extension and orientation angle to prior single molecule measurements; fractional extension distributions of linear and ring bead−spring chains with similar N_k (PDF)

Movie S1: K16 ring DNA tumbling in shear (AVI)

AUTHOR INFORMATION

Corresponding Author

Charles M. Schroeder − *Department of Materials Science and Engineering, Department of Chemical and Biomolecular Engineering, and Beckman Institute for Advanced Science and Technology, University of Illinois at Urbana−Champaign, Urbana, Illinois 61801, United States;* orcid.org/0000-0001-6023-2274; Email: cms@illinois.edu

Authors

Michael Q. Tu − *Department of Chemical and Biomolecular Engineering and Beckman Institute for Advanced Science and Technology, University of Illinois at Urbana−Champaign, Urbana, Illinois 61801, United States*

Megan Lee − *Department of Physics and Biophysics, University of San Diego, San Diego, California 92110, United States*

Rae M. Robertson-Anderson − *Department of Physics and Biophysics, University of San Diego, San Diego, California 92110, United States;* orcid.org/0000-0003-4475-4667

Complete contact information is available at: https://pubs.acs.org/10.1021/acs.macromol.0c01362

Notes

The authors declare no competing financial interest.

ACKNOWLEDGMENTS

This work was financially supported by the National Science Foundation (NSF) by Awards CBET-1604038 (M.Q.T. and C.M.S.) and CBET-1603925 (M.L. and R.M.R-A.) and the Joint Center for Energy Storage Research (JCESR), an Energy Innovation Hub funded by the U.S. Department of Energy, Office of Science, Basic Energy Sciences for M.Q.T. and C.M.S. The authors thank Charles Young, Charles Sing, and Gregory McKenna for useful discussions.

REFERENCES

(1) Rubinstein, M. Dynamics of Ring Polymers in the Presence of Fixed Obstacles. *Phys. Rev. Lett.* **1986**, *57*, 3023.

(2) McLeish, T. Polymers Without Beginning or End. *Science* **2002**, *297*, 2005−2006.

(3) De Gennes, P.-G.; Gennes, P.-G. *Scaling Concepts in Polymer Physics*; Cornell University Press: 1979.

(4) McLeish, T. Tube Theory of Entangled Polymer Dynamics. *Adv. Phys.* **2002**, *51*, 1379−1527.

(5) Hiemenz, P. C.; Lodge, T. P. *Polymer Chemistry*, 2nd ed.; CRC Press: 2007.

(6) Vinogradov, A. A.; Yin, Y.; Suga, H. Macrocyclic Peptides as Drug Candidates: Recent Progress and Remaining Challenges. *J. Am. Chem. Soc.* **2019**, *141*, 4167−4181.

(7) Wu, Q.; Rauscher, P. M.; Lang, X.; Wojtecki, R. J.; de Pablo, J. J.; Hore, M. J. A.; Rowan, S. J. Poly[n]catenanes: Synthesis of Molecular Interlocked Chains. *Science* **2017**, *358*, 1434−1439.

(8) Kaitz, J. A.; Diesendruck, C. E.; Moore, J. S. End Group Characterization of Poly (phthalaldehyde): Surprising Discovery of a Reversible, Cationic Macrocyclization Mechanism. *J. Am. Chem. Soc.* **2013**, *135*, 12755−12761.

(9) Lloyd, E. M.; Lopez Hernandez, H.; Feinberg, A. M.; Yourdkhani, M.; Zen, E. K.; Mejia, E. B.; Sottos, N. R.; Moore, J. S.; White, S. R. Fully Recyclable Metastable Polymers and Composites. *Chem. Mater.* **2019**, *31*, 398−406.

(10) Halverson, J. D.; Lee, W. B.; Grest, G. S.; Grosberg, A. Y.; Kremer, K. Molecular Dynamics Simulation Study of Nonconcatenated Ring Polymers in a Melt. I. Statics. *J. Chem. Phys.* **2011**, *134*, 204904.
(11) Halverson, J. D.; Lee, W. B.; Grest, G. S.; Grosberg, A. Y.; Kremer, K. Molecular Dynamics Simulation Study of Nonconcatenated Ring Polymers in a Melt. II. Dynamics. *J. Chem. Phys.* **2011**, *134*, 204905.
(12) Halverson, J. D.; Grest, G. S.; Grosberg, A. Y.; Kremer, K. Rheology of Ring Polymer Melts: From Linear Contaminants to Ring-linear Blends. *Phys. Rev. Lett.* **2012**, *108*, 038301.
(13) Takano, A.; Ohta, Y.; Masuoka, K.; Matsubara, K.; Nakano, T.; Hieno, A.; Itakura, M.; Takahashi, K.; Kinugasa, S.; Kawaguchi, D.; Takahashi, Y.; Matsushita, Y. Radii of Gyration of Ring-Shaped Polystyrenes with High Purity in Dilute Solutions. *Macromolecules* **2012**, *45*, 369−373.
(14) Gooßen, S.; Bras, A. R.; Pyckhout-Hintzen, W.; Wischnewski, A.; Richter, D.; Rubinstein, M.; Roovers, J.; Lutz, P. J.; Jeong, Y.; Chang, T.; Vlassopoulos, D. Influence of the Solvent Quality on Ring Polymer Dimensions. *Macromolecules* **2015**, *48*, 1598−1605.
(15) Roovers, J.; Toporowski, P. Synthesis of High Molecular Weight Ring Polystyrenes. *Macromolecules* **1983**, *16*, 843−849.
(16) McKenna, G.; Hadziioannou, G.; Lutz, P.; Hild, G.; Strazielle, C.; Straupe, C.; Rempp, P.; Kovacs, A. Dilute Solution Characterization of Cyclic Polystyrene Molecules and Their Zero-Shear Viscosity in the Melt. *Macromolecules* **1987**, *20*, 498−512.
(17) Lee, H. C.; Lee, H.; Lee, W.; Chang, T.; Roovers, J. Fractionation of Cyclic Polystyrene from Linear Precursor by HPLC at the Chromatographic Critical Condition. *Macromolecules* **2000**, *33*, 8119−8121.
(18) Kapnistos, M.; Lang, M.; Vlassopoulos, D.; Pyckhout-Hintzen, W.; Richter, D.; Cho, D.; Chang, T.; Rubinstein, M. Unexpected Power-Law Stress Relaxation of Entangled Ring Polymers. *Nat. Mater.* **2008**, *7*, 997−1002.
(19) Doi, Y.; Matsubara, K.; Ohta, Y.; Nakano, T.; Kawaguchi, D.; Takahashi, Y.; Takano, A.; Matsushita, Y. Melt Rheology of Ring Polystyrenes with Ultrahigh Purity. *Macromolecules* **2015**, *48*, 3140−3147.
(20) Pasquino, R.; Vasilakopoulos, T. C.; Jeong, Y. C.; Lee, H.; Rogers, S.; Sakellariou, G.; Allgaier, J.; Takano, A.; Bras, A. R.; Chang, T.; Gooßen, S.; Pyckhout-Hintzen, W.; Wischnewski, A.; Hadjichristidis, N.; Richter, D.; Rubinstein, M.; Vlassopoulos, D. Viscosity of Ring Polymer Melts. *ACS Macro Lett.* **2013**, *2*, 874−878.
(21) Doi, Y.; Matsumoto, A.; Inoue, T.; Iwamoto, T.; Takano, A.; Matsushita, Y.; Takahashi, Y.; Watanabe, H. Re-examination of Terminal Relaxation Behavior of High-Molecular-Weight Ring Polystyrene Melts. *Rheol. Acta* **2017**, *56*, 567−581.
(22) Yan, Z.-C.; Costanzo, S.; Jeong, Y.; Chang, T.; Vlassopoulos, D. Linear and Nonlinear Shear Rheology of a Marginally Entangled Ring Polymer. *Macromolecules* **2016**, *49*, 1444−1453.
(23) Huang, Q.; Ahn, J.; Parisi, D.; Chang, T.; Hassager, O.; Panyukov, S.; Rubinstein, M.; Vlassopoulos, D. Unexpected Stretching of Entangled Ring Macromolecules. *Phys. Rev. Lett.* **2019**, *122*, 208001.
(24) Michieletto, D.; Turner, M. S. A Topologically Driven Glass in Ring Polymers. *Proc. Natl. Acad. Sci. U. S. A.* **2016**, *113*, 5195−5200.
(25) Michieletto, D.; Nahali, N.; Rosa, A. Glassiness and Heterogeneous Dynamics in Dense Solutions of Ring Polymers. *Phys. Rev. Lett.* **2017**, *119*, 197801.
(26) Smrek, J.; Chubak, I.; Likos, C. N.; Kremer, K. Active Topological Glass. *Nat. Commun.* **2020**, *11*, 26.
(27) Schroeder, C. M. Single Polymer Dynamics for Molecular Rheology. *J. Rheol.* **2018**, *62*, 371−403.
(28) Perkins, T. T.; Smith, D.; Chu, S. Relaxation of a Single DNA Molecule Observed by Optical Microscopy. *Science* **1994**, *264*, 822−826.
(29) Smith, D. E.; Babcock, H. P.; Chu, S. Single-Polymer Dynamics in Steady Shear Flow. *Science* **1999**, *283*, 1724−1727.
(30) Teixeira, R. E.; Babcock, H. P.; Shaqfeh, E. S.; Chu, S. Shear Thinning and Tumbling Dynamics of Single Polymers in the Flow-Gradient Plane. *Macromolecules* **2005**, *38*, 581−592.
(31) Perkins, T. T.; Smith, D. E.; Chu, S. Single Polymer Dynamics in an Elongational Flow. *Science* **1997**, *276*, 2016−2021.
(32) Schroeder, C. M.; Shaqfeh, E. S.; Chu, S. Effect of Hydrodynamic Interactions on DNA Dynamics in Extensional Flow: Simulation and Single Molecule Experiment. *Macromolecules* **2004**, *37*, 9242−9256.
(33) Schroeder, C. M.; Babcock, H. P.; Shaqfeh, E. S.; Chu, S. Observation of Polymer Conformation Hysteresis in Extensional Flow. *Science* **2003**, *301*, 1515−1519.
(34) Hur, J. S.; Shaqfeh, E. S.; Babcock, H. P.; Smith, D. E.; Chu, S. Dynamics of Dilute and Semidilute DNA Solutions in the Start-up of Shear Flow. *J. Rheol.* **2001**, *45*, 421−450.
(35) Hsiao, K.; Sasmal, C.; Prakash, J. R.; Schroeder, C. M. Direct Observation of DNA Dynamics in Semi-dilute Solutions in Extensional Flow. *J. Rheol.* **2017**, *61*, 169−186.
(36) Sasmal, C.; Hsiao, K.; Schroeder, C. M.; Prakash, J. R. Parameter-free Prediction of DNA Dynamics in Planar Extensional Flow of Semi-dilute Solutions. *J. Rheol.* **2017**, *61*, 169−186.
(37) Teixeira, R.; Dambal, A. K.; Richter, D. H.; Shaqfeh, E. S. G.; Chu, S. The Individualistic Dynamics of Entangled DNA in Solution. *Macromolecules* **2007**, *40*, 2461−2476.
(38) Zhou, Y.; Schroeder, C. M. Dynamically Heterogeneous Relaxation of Entangled Polymer Chains. *Phys. Rev. Lett.* **2018**, *120*, 267801.
(39) Laib, S.; Robertson, R. M.; Smith, D. E. Preparation and Characterization of a Set of Linear DNA Molecules for Polymer Physics and Rheology Studies. *Macromolecules* **2006**, *39*, 4115−4119.
(40) Smith, D. E.; Perkins, T. T.; Chu, S. Dynamical Scaling of DNA Diffusion Coefficients. *Macromolecules* **1996**, *29*, 1372−1373.
(41) Robertson, R. M.; Laib, S.; Smith, D. E. Diffusion of Isolated DNA Molecules: Dependence on Length and Topology. *Proc. Natl. Acad. Sci. U. S. A.* **2006**, *103*, 7310−7314.
(42) Robertson, R. M.; Smith, D. E. Strong Effects of Molecular Topology on Diffusion of Entangled DNA Molecules. *Proc. Natl. Acad. Sci. U. S. A.* **2007**, *104*, 4824−4827.
(43) Robertson, R. M.; Smith, D. E. Self-diffusion of Entangled Linear and Circular DNA Molecules: Dependence on Length and Concentration. *Macromolecules* **2007**, *40*, 3373−3377.
(44) Chapman, C. D.; Shanbhag, S.; Smith, D. E.; Robertson-Anderson, R. M. Complex Effects of Molecular Topology on Diffusion in Entangled Biopolymer Blends. *Soft Matter* **2012**, *8*, 9177−9182.
(45) Li, Y.; Hsiao, K.-W.; Brockman, C. A.; Yates, D. Y.; Robertson-Anderson, R. M.; Kornfield, J. A.; San Francisco, M. J.; Schroeder, C. M.; McKenna, G. B. When Ends Meet: Circular DNA Stretches Differently in Elongational Flows. *Macromolecules* **2015**, *48*, 5997−6001.
(46) Hsiao, K.-W.; Schroeder, C. M.; Sing, C. E. Ring Polymer Dynamics Are Governed by a Coupling Between Architecture and Hydrodynamic Interactions. *Macromolecules* **2016**, *49*, 1961−1971.
(47) Zhou, Y.; Hsiao, K. W.; Regan, K. E.; Kong, D.; McKenna, G. B.; Robertson-Anderson, R. M.; Schroeder, C. M. Dynamics of Single Ring Polymers in Semi-dilute Linear Polymer Solutions. *Nat. Commun.* **2019**, *10*, 1753.
(48) Romero, O.; Scriven, L.; Carvalho, M. Slot Coating of Mildly Viscoelastic Liquids. *J. Non-Newtonian Fluid Mech.* **2006**, *138*, 63−75.
(49) Stone, H. A.; Stroock, A. D.; Ajdari, A. Engineering Flows in Small Devices: Microfluidics Toward a Lab-on-a-Chip. *Annu. Rev. Fluid Mech.* **2004**, *36*, 381−411.
(50) Babcock, H. P.; Smith, D. E.; Hur, J. S.; Shaqfeh, E. S.; Chu, S. Relating the Microscopic and Macroscopic Response of a Polymeric Fluid in a Shearing Flow. *Phys. Rev. Lett.* **2000**, *85*, 2018.
(51) Schroeder, C. M.; Teixeira, R. E.; Shaqfeh, E. S.; Chu, S. Dynamics of DNA in the Flow-Gradient Plane of Steady Shear Flow: Observations and Simulations. *Macromolecules* **2005**, *38*, 1967−1978.

https://dx.doi.org/10.1021/acs.macromol.0c01362
Macromolecules 2020, 53, 9406−9419

(52) Schroeder, C. M.; Teixeira, R. E.; Shaqfeh, E. S.; Chu, S. Characteristic Periodic Motion of Polymers in Shear Flow. *Phys. Rev. Lett.* **2005**, *95*, 018301.
(53) Cifre, J. H.; Pamies, R.; Martínez, M. L.; de la Torre, J. G. Steady-state Behavior of Ring Polymers in Dilute Flowing Solutions via Brownian Dynamics. *Polymer* **2005**, *46*, 267−274.
(54) Chen, W.; Chen, J.; An, L. Tumbling and Tank-Treading Dynamics of Individual Ring Polymers in Shear Flow. *Soft Matter* **2013**, *9*, 4312−4318.
(55) Liebetreu, M.; Ripoll, M.; Likos, C. N. Trefoil Knot Hydrodynamic Delocalization on Sheared Ring Polymers. *ACS Macro Lett.* **2018**, *7*, 447−452.
(56) Young, C. D.; Qian, J. R.; Marvin, M.; Sing, C. E. Ring Polymer Dynamics and Tumbling-Stretch Transitions in Planar Mixed Flows. *Phys. Rev. E: Stat. Phys., Plasmas, Fluids, Relat. Interdiscip. Top.* **2019**, *99*, 062502.
(57) Kundukad, B.; Yan, J.; Doyle, P. S. Effect of YOYO-1 on the Mechanical Properties of DNA. *Soft Matter* **2014**, *10*, 9721−9728.
(58) Marko, J. F.; Siggia, E. D. Stretching DNA. *Macromolecules* **1995**, *28*, 8759−8770.
(59) Selvin, P. R.; Ha, T. *Single-Molecule Techniques*; Cold Spring Harbor Laboratory Press: 2008.
(60) Deschamps, J.; Kantsler, V.; Steinberg, V. Phase Diagram of Single Vesicle Dynamical States in Shear Flow. *Phys. Rev. Lett.* **2009**, *102*, 118105.
(61) Anthony, S.; Zhang, L.; Granick, S. Methods to Track Single-Molecule Trajectories. *Langmuir* **2006**, *22*, 5266−5272.
(62) Chen, K.; Anthony, S. M.; Granick, S. Extending Particle Tracking Capability with Delaunay Triangulation. *Langmuir* **2014**, *30*, 4760−4766.
(63) Anczurowski, E.; Mason, S. The Kinetics of Flowing Dispersions: II. Equilibrium Orientations of Rods and Discs (Theoretical). *J. Colloid Interface Sci.* **1967**, *23*, 522−532.
(64) Harasim, M.; Wunderlich, B.; Peleg, O.; Kröger, M.; Bausch, A. R. Direct Observation of the Dynamics of Semiflexible Polymers in Shear Flow. *Phys. Rev. Lett.* **2013**, *110*, 108302.
(65) Gerashchenko, S.; Steinberg, V. Statistics of Tumbling of a Single Polymer Molecule in Shear Flow. *Phys. Rev. Lett.* **2006**, *96*, 038304.
(66) Zhou, Y.; Schroeder, C. M. Single polymer dynamics under large amplitude oscillatory extension. *Physical Review Fluids* **2016**, *1*, 053301.
(67) Öttinger, H. C. *Stochastic Processes in Polymeric Fluids: Tools and Examples for Developing Simulation Algorithms*; Springer Science & Business Media: 1996.
(68) Rotne, J.; Prager, S. Variational treatment of hydrodynamic interaction in polymers. *J. Chem. Phys.* **1969**, *50*, 4831−4837.
(69) Prakash, J. R. Rouse chains with excluded volume interactions in steady simple shear flow. *J. Rheol.* **2002**, *46*, 1353−1380.
(70) Liebetreu, M.; Likos, C. N. Hydrodynamic Inflation of Ring Polymers under Shear. *Commun. Mater.* **2020**, *1*, 1−11.
(71) Wang, Z.; Zhai, Q.; Chen, W.; Wang, X.; Lu, Y.; An, L. Mechanism of Nonmonotonic Increase in Polymer Size: Comparison between Linear and Ring Chains at High Shear Rates. *Macromolecules* **2019**, *52*, 8144−8154.

https://dx.doi.org/10.1021/acs.macromol.0c01362
Macromolecules 2020, 53, 9406−9419